Single-Molecule Conductance of a π-Hybridized Tripodal Anchor while Maintaining Electronic Communication

Tatsuhiko Ohto, Aya Tashiro, Takuji Seo, Nana Kawaguchi, Yuichi Numai, Junpei Tokumoto, Soichiro Yamaguchi, Ryo Yamada*, Hirokazu Tada*, Yoshio Aso*, and Yutaka Ie**

Dr. T. Ohto, Y. Numai, J. Tokumoto, S. Yamaguchi, Prof. R. Yamada, Prof. H. Tada
Graduate School of Engineering Science, Osaka University, 1-3 Machikaneyama, Toyonaka, Osaka 560-8531, Japan
E-mail: ohto@molectronics.jp, yamada@molectronics.jp, tada@molectronics.jp, aso@sanken.osaka-u.ac.jp, yutakaie@sanken.osaka-u.ac.jp

A. Tashiro, T. Seo, N. Kawaguchi, Prof. Y. Aso, Prof. Y. Ie
The Institute of Scientific and Industrial Research (ISIR), Osaka University, 8-1 Mihogaoka, Ibaraki, Osaka 567-0047, Japan

Keywords: single-molecule electronics, tripodal anchor, structure-property relationship, π-channel hybridization, unsupervised clustering, NEGF-DFT

Direct hybridization between the π-orbital of a conjugated molecule and metal electrodes is recognized as a new anchoring strategy to enhance the electrical conductance of single-molecule junctions. The anchor is expected to maintain direct hybridization between the conjugated molecule and the metal electrodes, and control the orientation of the molecule against the metal electrodes. However, fulfilling both the requirements is difficult because multipodal anchors aiming at a robust contact with the electrodes often break the π-conjugation, thereby resulting in an inefficient carrier transport. Herein, a new tripodal anchor framework— a 7,7-diphenyl-7*H*-benzo[6,7]indeno[1,2-*b*]thiophene (**PBIT**) derivative— is developed. In this framework, π-conjugation is maintained in the molecular junction, and the tripodal structure makes the molecule stand upright on the metal electrode. Molecular conductance is measured by the break junction technique. A vector-based classification and first-principles transport calculations determine the single-molecule conductance of the tripodal-anchoring structure. The conductance of the **PBIT**-based molecule is higher than that of the tripodal anchor having sp^3 carbon atoms in the carrier transport pathway. These results

demonstrate that extending the π-conjugation to the tripodal leg is an effective strategy for enhancing the conductivities of single-molecule junctions.

1. Introduction

Single-molecule electronics has been studied for next-generation devices because of its possible bottom-up construction and potential for device miniaturization.[1-8] The development of an anchor for connecting between organic molecules and metal electrodes is of significant importance to control the charge-transport characteristics of metal-molecule-metal junctions.[9] Although the most widely used anchor to connect organic molecules and Au electrodes is a thiol (–SH) group that forms an S–Au bond,[10, 11] it was found that the S–Au bond is not suitable for realizing a strong coupling between the π-orbitals in an organic molecule and metal electrodes.[12] Recently, a new anchoring strategy that utilizes direct hybridization between the π-orbitals of a conjugated molecule and metal electrodes (π-channel hybridization) has been reported to exhibit high conductance.[13-17] However, the development of the anchors for the π-channel hybridization still insufficient because the difficulty of molecular design that fulfills (1) the direct hybridization between the π-orbital of a conjugated molecule and metal electrodes, (2) the control of molecular orientation against the metal electrodes, and (3) the formation of a π-channel from one metal electrode to another through the extended π-conjugation in the molecule.

We have recently established a rational design principle to fulfill points (1) and (2), mentioned above. The combination of a tripodal tetraphenylmethane framework with aromatic rings such as pyridine and thiophene as the anchoring functional groups is an effective molecular design to realize a stable single-molecule junction through the direct hybridization of the π-orbital to metal electrodes.[18, 19] The tripodal structure with electron-rich thiophene rings, **3Th** (**Figure 1**), exhibited excellent adsorption on Au(111) substrates, and the bistripodal compound **3Th-Ph-3Th** exhibited hole-transporting characteristics in the

single-molecule junction.[19] However, the π-orbital in the molecule was not completely connected because of the presence of a methane sp^3 carbon atom in tetraphenylmethane.

In this study, to accomplish all the requirements mentioned in points (1)–(3), we developed a 7,7-diphenyl-7*H*-benzo[6,7]indeno[1,2-*b*]thiophene framework (**PBIT**) with the thiophene rings (**Th**) acting as the anchoring functional groups. Further, we also developed a **PBIT(3Th)**-based tripodal compound— **PBIT(3Th)-A-PBIT(3Th)** (Figure 1) — in which the π-conjugation is extended from the acetylene linker (**A)** to one of the tripodal legs. The electrical conductance and current–voltage (*I*–*V*) curves of the single-molecule **PBIT(3Th)-A-PBIT(3Th)** junctions were measured using the mechanically controllable break junction (MCBJ) method. The vector-based classification of the measured *I*–*V* curves indicated the presence of three types of molecular junction structures that are distinguished by the conductance and contact asymmetry. Plausible models for the single-molecule junctions corresponding to each structure were proposed on the basis of first-principles calculations. In these structures, a π-channel is formed from one electrode to the other through the extended π-conjugation in the molecule.

2. Results and Discussion

2.1. Gas-Phase Calculation

We estimated the optimized structures and molecular orbitals of **3Th-Ph-3Th** and **PBIT(3Th)-A-PBIT(3Th)** using the density functional theory (DFT) calculations at the B3LYP/6-31G(d,p) level of theory. As shown in Figure 1, these molecules showed three-dimensional structures, which are expected to have desired molecular orientations on the metal electrodes. The highest occupied molecular orbital (HOMO) of the hole-transporting[19] **3Th-Ph-3Th** is localized on the "leg" part of the **3Th** unit. On the other hand, **PBIT(3Th)-A-PBIT(3Th)** possess delocalized HOMO orbital entirely over the π-conjugated backbone.

Because of this delocalization, the HOMO level becomes higher for **PBIT(3Th)-A-PBIT(3Th)** (–5.02 eV) than that for **3Th-Ph-3Th** (–5.58 eV), which may induce higher conductance (Figure 1). These results indicate that the **PBIT** framework is effective in considering three-dimensional structures and maintaining intramolecular electronic communication.

2.2. Synthesis

The synthesis scheme of **PBIT(3Th)-A-PBIT(3Th)** is presented in **Scheme 1**. Compound **2** was readily synthesized via the Suzuki coupling reaction between boronic ester **1** and methyl 2-bromothiophene-3-carboxylate. Further, compound **2** was reacted with 4-lithiobromobenzene (formed in situ by the reaction between 1,4-dibromobenzene and *n*-BuLi), which was then treated with trifluoromethanesulfonic acid (TfOH) to give tripodal compound **3**. Selective bromination of compound **3** at α position in the thiophene ring gave tribromo compound **4**, which was subjected to a Stille coupling reaction with 2-tributylstannylthiophene to give key intermediate compound **5**. The methoxy group in compound **5** was successfully converted to triflate and trimethylsilyl (TMS) acetylene groups to synthesize compounds **i-c** and **6**, respectively. Finally, the Sonogashira–Hagihara coupling reaction between **i-c** and TMS-deprotected compound **6** produced the target compound **PBIT(3Th)-A-PBIT(3Th)**. Since these molecules showed sufficient solubility toward chloroform ($CHCl_3$) owing to their three-dimensional structures, the chemical structures were fully characterized using nuclear magnetic resonance (NMR) spectroscopy, mass spectroscopy (MS), and high-resolution MS. The NMR spectra are shown in the Supporting Information (SI).

2.3. Measurements of Electrical Conductance

The *I*–*V* characteristics and conductance of the single-molecule junctions of **PBIT(3Th)-A-PBIT(3Th)** were measured using MCBJ method[20] at 80 K. As shown in **Figure 2**(a), a small Au contact was prepared on an elastic substrate made of phosphor bronze that was covered with polyimide. A pushing rod was moved to bend the substrate, which was fixed in a three-point bending geometry. As a result of the substrate bending, the Au contact was elongated and broken. Using this three-point bending geometry, the distance between two electrodes can be controlled with a picometer precision. To modify the **PBIT(3Th)-A-PBIT(3Th)** molecules on the electrodes, a droplet of a 0.1 mM solution of the molecules in $CHCl_3$ was placed on the substrate such that the Au contact remained covered. The distance between the electrodes was changed by ~0.04 nm by moving the pushing rod using a piezoelectric stepper motor. The *I*–*V* characteristics were measured at every step of the piezoelectric stepper motor. A histogram analysis was performed to determine the conductance for a single-molecule junction. The conductance of the molecules was determined from the current value at V_{bias} = 100 mV. Figure 2(b) shows the conductance histogram for **PBIT(3Th)-A-PBIT(3Th)** with the Au electrodes, obtained from 32,346 *I*–*V* curves measured during the breaking process. The arrows in the figure indicate the peak positions that correspond to the molecular conductance values, which were found to be $1 \times 10^{-2}\ G_0$ and $1 \times 10^{-4}\ G_0$ ($G_0 = 2e^2\ h^{-1}$, where *e* and *h* are the elemental charge and Plank's constant, respectively). These conductance values are higher than those obtained for **3Th-Ph-3Th** ($2 \times 10^{-5}\ G_0$),[19] indicating that tripodal anchor unit with the effective π-conjugation through the π-channel hybridization enhanced the conductance.

2.4. Analysis of the Characteristics of the *I*–*V* Curves

Since the conductance histogram exhibited multiple peaks, we applied vector-based clustering, which has been applied for the conductance traces of the break junction methods,[21, 22] to classify the *I*–*V* curves. For the classification, an *i*th *I*–*V* curve with *N* data

points was defined as an N-dimensional vector $\mathbf{I}_i$. We also defined an N-dimensional reference vector, **R**, as the averaged I–V curve. Unsupervised clustering was performed using ΔX_i and θ_i, where ΔX_i is the norm of the vector $\mathbf{I}_i - \mathbf{R}$ and θ_i is the angle between **R** and $\mathbf{R} - \mathbf{I}_i$. Further details can be found in Experimental Section. This classification method facilitates classifying the data based on the differences in the shape of the curves, which is helpful in analyzing various I–V curves obtained from the MCBJ measurements.

An unsupervised clustering was performed for 32,346 I–V curves using the k-means clustering method[21], and the number of clusters, i.e., the parameter k, was set to 4. As shown in **Figure 3**(a), the distribution of ΔX and θ is classified into four clusters according to ΔX. We name this as cluster 1, cluster 2, cluster 3, and cluster 4 in the ascending order of the values of ΔX. Figure 3(b) shows the conductance histogram for cluster 1 and the average of the I–V curves corresponding to cluster 1. The average of all the I–V curves, **R**, is also shown for comparison. Cluster 1 exhibits a conductance peak at ~1×10^{-2} G_0, which explains the highest peak (1×10^{-2} G_0) observed in the total conductance histogram (Figure 1(b)). The averaged I–V curve of cluster 1 is symmetric and has the smallest deviation from **R**. Therefore, we conclude that the molecular junctions represented by cluster 1 show a symmetric I–V curve with high conductance; we categorize cluster 1 as "sym-HC". As shown in Figure 3(c), cluster 2 exhibits a lower conductance peak (1×10^{-4} G_0) than that of the cluster 1, while the averaged I–V curve of cluster 2 is symmetric; hence, cluster 2 is categorized as "sym-LC". Figure 3(d) shows that the peak position in the conductance histogram of cluster 3 is close to that of cluster 2 (1×10^{-4} G_0). However, the averaged I–V curve is asymmetric with the rectification ratio of 2.5 at 1.5 V. Thus, we categorize cluster 3 as "asym-LC". Since the peak conductance of the conductance histogram of cluster 4 is very low (Figure 3(e)) and the averaged I–V curve of cluster 4 indicates the absence of molecules between the metal electrodes, cluster 4 is categorized as a "broken" junction.

These results indicate that at least three distinct molecular junction structures that are present are characterized by the conductance value and the symmetricity of the *I*–*V* curve. Since the symmetry of the *I*–*V* curve originates from the symmetry of the electronic coupling between the molecular orbitals and the two electrodes that are in contact with the molecule (see the SI),[23] we can conclude that there are at least three types of anchoring structures (two symmetrical and one asymmetrical).

2.5. First-Principles Transport Calculations

Based on the symmetric and asymmetric *I*–*V* curves obtained from k-means clustering, we assumed two series of potential energy surfaces (PESs) and calculated the molecular binding energy by changing the electrode gap length, as shown in **Figure 4**(a). On one PES (PES1), both the tripodal anchors were symmetrically self-standing on the Au surfaces. PES1 has a deep minimum, where the **PBIT(3Th)-A-PBIT(3Th)** achieves the self-standing structure. The transmission coefficient (Figure 4(b)) of this structure indicates that the HOMO level is at –0.74 eV, which is higher than that of **3Th-Ph-3Th** (–1.28 eV) (Figure S1), because of the effective intramolecular π-channel hybridization. On the other PES (PES2), one of the tripodal anchors was laid on its side and there are several minima. These structures would appear during the formation of molecular junctions after the contact of two electrodes.

Based on the calculated conductance values, these molecular junction structures can be qualitatively categorized into the clusters obtained by vector-based classification. On PES2, **PBIT(3Th)-A-PBIT(3Th)** formed asymmetric structures, except for the most stable point at the short electrode gap distance. At the most stable point, the whole molecule strongly interacted with the electrodes, thereby giving a conductance value higher than 1 G_0. When the surface of the electrode was heterogeneous, the conductance value decreased to 0.1 G_0, which is reasonable considering the estimation of the high conductance peak, at 1×10^{-2} G_0, that is observed in the experiment (see the SI). Hence, this structure corresponds to cluster 1. PES2

contained several local minima, where one of the π-conjugated leg on one side of the anchors was parallel to the electrode surface. These asymmetric molecular junction structures on PES2 gave conductance values on the order of 1×10^{-4} G_0, which agrees well with the low conductance peak (1×10^{-4} G_0) observed in the experiment. These asymmetric structures with low conductance values were included in cluster 3. Cluster 2 can be attributed to the structure at the optimal electrode gap distance on PES1 because it gave a low conductance value, and no other symmetric structures giving low conductance values were observed. The calculated conductance value (1.4×10^{-5} G_0) of the self-standing structure was smaller than the experimental value, which can be attributed to a heterogeneous electrode surface in the experiment. As shown above, the plausible molecular junction structures were predicted by combining vector-based classification and first-principles transport calculations. This strategy will be useful for determining the various molecular junction structures from a large number of *I*–*V* curves.

The theoretical analysis revealed that the self-standing structure and robust metal-molecule contact are achieved in the sym-LC structure (cluster 2). The MCBJ measurements and theoretical calculations showed that the conductance of **PBIT(3Th)-A-PBIT(3Th)** is higher than that of **3Th-Ph-3Th**,[19] because of the higher HOMO level through the effective intramolecular π-channel hybridization.

3. Conclusion

To summarize, we designed and synthesized a new tripodal anchor unit based on 7,7-diphenyl-7*H*-benzo[6,7]indeno[1,2-*b*]thiophene framework and thiophene rings to accomplish the hybridization of the π-orbital with Au electrodes and hole transport through π-conjugation. Further, the single-molecule conductance of a π-conjugated molecule having the new anchors was measured using the MCBJ technique. The vector-based classification

revealed the presence of at least three types of molecular junction structures distinguished by their conductance and contact asymmetries. The first-principles transport calculations suggested that one of those structures (sym-LC) achieved the self-standing anchoring between the molecule and the metal electrodes. It has been determined that the newly developed tripodal anchor molecule shows a higher conductance than a previous tripodal anchor molecule having sp^3 carbon atoms in the carrier transport pathway. To our knowledge, this is the first report on a tripodal anchor unit with effective π-conjugation through π-channel hybridization. We found that our newly developed tripodal anchor not only achieves a self-standing and robust molecule–metal junction, but also shows the various molecular junction structures and high conductance values through π-channel hybridization. Therefore, the development of molecular systems, including this anchor unit to realize single-molecule electronics, is targeted in our group.

4. Experimental Section

4.1. Synthesis and Characterization of Molecules

Column chromatography was performed on silica gel, KANTO Chemical silica gel 60N (40–50 μm). Thin-layer chromatography plates were visualized with UV light. Preparative gel-permeation chromatography (GPC) was performed on a Japan Analytical Industry LC-918 equipped with JAI-GEL 1H/2H. Melting points are uncorrected. ^{1}H and ^{13}C NMR spectra were recorded on a JEOL ECS-400 spectrometer in $CDCl_3$ with tetramethylsilane (TMS) as an internal standard. Data are reported as follows: chemical shift in ppm (δ), multiplicity (s = singlet, d = doublet, t = triplet, m = multiplet), coupling constant (Hz), and integration. Mass spectra were obtained on a Shimadzu AXIMA-TOF. Elemental analyses were performed on Perkin Elmer LS-50B by the Elemental Analysis Section of comprehensive analysis center (CAC), ISIR, Osaka University.

*Synthesis of **2***: **1** (1.28 g, 4.50 mmol), methyl 2-bromothiophene-3-carboxylate (1.49 g, 6.74 mmol), K_2CO_3 (1.86 g, 13.50 mmol), and $Pd(PPh_3)_4$ (519 mg, 0.45 mmol) were placed in a test tube with screw cap and dissolved with toluene (30 mL), EtOH 1.5 mL), and H_2O (6 mL). The reaction mixture was refluxed for overnight. After being cooled to room temperature and addition of water, the resulting mixture was extracted with diethyl ether (Et_2O), and the organic layer was washed with brine and dried over Na_2SO_4. The combined organic layer was concentrated under reduced pressure and then purified by column chromatography on silica gel (hexane:CH_2Cl_2 = 1:1~2:3) to give **2** as a white solid (1.32 g, 98%). ^{1}H NMR (400 MHz, $CDCl_3$, TMS, δ): 7.79 (d, J = 8.4 Hz, 1H), 7.61 (d, J = 5.6 Hz, 1H), 7.52 (d, J = 9.2 Hz, 1H), 7.46 (t, J = 7.8 Hz, 1H), 7.36 (d, J = 5.6 Hz, 1H), 7.33 (dd, J = 7.2, 1.2 Hz, 1H), 7.18 (d, J = 2.8 Hz, 1H), 7.08 (dd, J = 9.2, 2.4 Hz, 1H), 3.93 (s, 3H), 3.50 (s, 3H); ^{13}C NMR (100 MHz, $CDCl_3$, δ): 163.3, 157.5, 148.9, 134.5, 131.2, 130.4, 129.1, 128.0, 127.1, 125.8, 125.4, 124.7, 119.1, 106.1, 55.3, 51.5; MS (MALDI) *m/z* 298.65. HRMS (APCI) *m/z*: $[M]^+$ calcd for $C_{17}H_{14}O_3S$, 298.0664; found, 298.0655.

*Synthesis of **3***: 1,4-Dibromobenzene (2.26 g, 9.64 mmol) and THF (16 mL) was placed in a 100 mL round-bottomed flask. To the mixture was added dropwise *n*-BuLi (1.64 M, 5.88 mL, 9.64 mmol) at –78 °C. After stirring for 1 h, **2** (870 mg, 2.92 mmol) in THF (5.5 mL) was added, and the mixture was allowed to warm to 0 °C for 2 h. Then, the reaction was quenched by the addition of ice. The aqueous layer was extracted with ethyl acetate (EtOAc), and the combined organic layer was washed with 2N HCl aq. and water and dried over Na_2SO_4. After removal of the solvent under reduced pressure, the residue was purified by column chromatography on silica gel (CH_2Cl_2) to give intermediate **i-a** (1.69 g, 99%). ^{1}H NMR (400 MHz, $CDCl_3$, TMS, δ): 7.68 (d, J = 8.8 Hz, 1H), 7.46 (d, J = 9.2 Hz, 1H), 7.31-7.33 (m, 3H),

7.21-7.26 (m, 4H), 7.09 (d, *J* = 2.4 Hz, 1H), 6.96-7.06 (m, 5H), 6.68 (d, *J* = 5.6 Hz, 1H), 3.93 (s, 3H), 2.67 (s, 1H). This compound was used without further purification.

Intermediate **i-a** (1.65 g, 2.84 mmol) was placed in a round-bottomed flask and dissolved with toluene (30 mL). To the mixture was added trifluoromethanesulfonic acid (TfOH) (20 drops) at room temperature. After stirring for 0.5 h, the reaction was quenched by the addition of ice. The aqueous layer was extracted with toluene and dried over Na_2SO_4. After removal of the solvent under reduced pressure, the residue was purified by column chromatography on silica gel (hexane:CH_2Cl_2 = 1:1) to give **3** as a brown solid (1.37 g, 83%, 2 steps). ^{1}H NMR (400 MHz, $CDCl_3$, TMS, δ): 8.09 (d, *J* = 9.2 Hz, 1H), 7.61 (d, *J* = 8.8 Hz, 1H), 7.43 (d, *J* = 5.2 Hz, 1H), 7.39 (d, *J* = 8.0 Hz, 1H), 7.34 (d, *J* = 8.8 Hz, 4H), 7.30 (dd, *J* = 9.2, 2.8 Hz, 1H), 7.19 (d, *J* = 2.0 Hz, 1H), 7.09 (d, *J* = 8.4 Hz, 4H), 7.04 (d, *J* = 4.8 Hz, 1H), 3.95 (s, 3H); ^{13}C NMR (100 MHz, $CDCl_3$, δ): 157.9, 155.3, 147.7, 143.0, 140.5, 134.6, 133.7, 131.6, 131.4, 129.7, 129.6, 129.0, 128.5, 127.9, 126.1, 125.4, 124.0, 122.2, 122.1, 121.1, 119.6, 106.6, 62.7, 54.4; MS (MALDI) *m/z* 561.96. HRMS (APCI) *m/z*: $[M+H]^+$ calcd for $C_{28}H_{18}Br_2OS$, 559.9445; found, 560.9505.

*Synthesis of **4***: To a stirred solution of **3** (1.41 g, 2.51 mmol) in $CHCl_3$ (15 mL) was added NBS (536 mg, 3.01 mmol) at 0 ºC. After stirring at 0 ºC for 0.5 h, the precipitate was filtered and washed with cool $CHCl_3$ to give **4** as a white solid (1.31 g, 81%). ^{1}H NMR (400 MHz, $CDCl_3$, TMS, δ): 7.90 (d, *J* = 9.2 Hz, 1H), 7.62 (d, *J* = 8.8 Hz, 1H), 7.35-7.38 (m, 5H), 7.28-7.31 (m, 1H), 7.19 (d, *J* = 2.8 Hz, 1H), 7.05-7.07 (m, 5H), 3.95 (s, 3H); ^{13}C NMR (100 MHz, $CDCl_3$, δ): 158.1, 154.0, 146.7, 142.3, 140.8, 134.7, 133.4, 131.7, 131.6, 129.6, 129.5, 128.6, 127.8, 125.9, 125.7, 125.5, 125.2, 124.1, 123.8, 121.8, 121.3, 119.8, 114.9, 106.8, 63.6, 55.4; MS (MALDI) *m/z* 641.30 (M^+, Calcd 641.22). Anal. calcd for $C_{28}H_{17}Br_3OS$: C 52.45, H 2.67, N 0.00; found: C 52.49, H 2.94, N 0.00.

*Synthesis of **5***: **4** (480 mg, 0.75 mmol), 2-tributylstannylthiophene (1.26 g, 3.38 mmol), and $Pd(PPh_3)_4$ (129 mg, 0.112 mmol) were placed in a microtube and dissolved with toluene (15 mL). The mixture was then reacted in a microwave reactor at 180 °C for 10 min. After being cooled to room temperature, the reaction mixture was filtered over celite with toluene as an eluent, and then purified by column chromatography on silica gel (hexane:CH_2Cl_2 = 2:1) to give **5** as a yellow solid (339 mg, 69%). Further purification was performed by recrystallization using hexane and CH_2Cl_2. ^{1}H NMR (400 MHz, $CDCl_3$, TMS, δ): 8.08 (d, J = 8.8 Hz, 1H), 7.62 (d, J = 8.4 Hz, 1H), 7.48-7.51 (m, 5H), 7.21-7.32 (m, 13H), 7.02-7.05 (m, 3H), 3.95 (s, 3H); ^{13}C NMR (100 MHz, $CDCl_3$, δ): 157.9, 156.4, 148.1, 144.0, 143.0, 141.1, 139.0, 137.9, 134.6, 133.7, 133.2, 128.5, 128.0, 127.9, 126.2, 126.1, 125.3, 124.8, 124.4, 124.2, 123.4, 123.0, 122.0, 119.4, 119.0, 106.7, 63.6, 55.4; MS (MALDI) *m/z* 650.48 (M^+, Calcd 650.89). HRMS (APCI) *m/z*: $[M]^+$ calcd for $C_{40}H_{26}OS_4$, 650.0866; found, 650.0853.

*Synthesis of **6***: To a stirred solution of **5** (1.04 g, 1.60 mmol) in CH_2Cl_2 (50 mL) was added BBr_3 (6.4 mL, 1.0 M CH_2Cl_2 solution) at –78 °C, and the resulting mixture was stirred at 0 °C for 1 h. The reaction was quenched by the addition of ice. The aqueous layer was extracted with CH_2Cl_2 and dried over Na_2SO_4. After removal of the solvent under reduced pressure, the residue was passed through short column chromatography on silica gel (CH_2Cl_2) to give phenol intermediate **i-b** as a yellow solid (602 mg). ^{1}H NMR (400 MHz, $CDCl_3$, TMS, δ): 8.10 (d, J = 8.4 Hz, 1H), 7.56 (d, J = 8.0 Hz, 1H), 7.48-7.51 (m, 5H), 7.22-7.30 (m, 13H), 7.02-7.05 (m, 3H), 4.97 (s, 1H). This compound was used without further purification.

To a stirred solution of **i-b** (550 mg, 0.864 mmol) and NEt_3 (262 mg, 2.59 mmol) in CH_2Cl_2 (55 mL) was added trifluoroacetic anhydride (Tf_2O) (293 mg, 1.04 mmol) at 0 ºC. After stirring at 0 ºC for 1 h, sat. $NaHCO_3$ aq. was added, and the resulting mixture was extracted with CH_2Cl_2, and the organic layer was washed with brine and dried over Na_2SO_4. The combined organic layer was concentrated under reduced pressure and then purified by

column chromatography on silica gel (hexane:CH_2Cl_2 = 1:1) to give intermediate **i-c** as a yellow solid (628 mg, 56%, 2 steps). ^{1}H NMR (400 MHz, $CDCl_3$, TMS, δ): 8.26 (d, J = 8.8 Hz, 1H), 7.81 (d, J = 2.8 Hz, 1H), 7.75 (d, J = 8.4 Hz, 1H), 7.65 (d, J = 8.4 Hz, 1H), 7.50-7.54 (m, 5H), 7.23-7.30 (m, 11H), 7.04-7.06 (m, 3H), 4.97 (s, 1H). This compound was used without further purification.

Intermediate **i-c** (474 mg, 0.616 mmol), trimethysilylacetylene (303 mg, 3.08 mmol), CuI (12 mg, 0.062 mmol), PPh_3 (32 mg, 0.123 mmol), and $Pd(PPh_3)_4$ (72 mg, 0.062 mmol) were placed in a test tube with screw cap and dissolved with piperidine (16 mL), and the resulting mixture was stirred at 110 ºC for 12 h. After being cooled to room temperature, the reaction mixture was filtered over celite with $CHCl_3$ as an eluent. After removal of the solvent under reduced pressure, the residue was purified by column chromatography on silica gel (hexane:CH_2Cl_2 = 2:1) to give **6** as a yellow solid (336 mg, 76%).^{1}H NMR (400 MHz, $CDCl_3$, TMS, δ): 8.08 (d, J = 8.8 Hz, 1H), 8.05 (s, 1H), 7.63-7.68 (m, 2H), 7.55 (d, J = 8.4 Hz, 1H), 7.48-7.51 (m, 4H), 7.22-7.31 (m, 11H), 7.03-7.06 (m, 3H), 0.30 (s, 9H); ^{13}C NMR (100 MHz, $CDCl_3$, δ): 156.5, 151.1, 143.8, 142.5, 141.5, 138.5, 137.7, 133.8, 133.4, 132.7, 129.3, 128.5, 128.0, 127.9, 126.3, 126.1, 125.8, 124.8, 124.6, 124.5, 124.3, 123.6, 123.1, 120.8, 118.9, 105.2, 95.1, 63.8, 0.00; MS (MALDI) *m/z* 717.36 (M^+, Calcd 717.07). Anal. calcd for $C_{44}H_{32}S_4Si$: C 73.70, H 4.50, N 0.00; found: C 73.81, H 4.74, N 0.00.

Synthesis of ***PBIT(3Th)-A-PBIT(3Th)***: To a stirred solution of **6** (286 mg, 0.400 mmol) in THF (16 mL) was added TBAF (1.2 mL, 1.0 M THF solution) at 0 °C. After stirring at 0 °C for 1 h, the reaction was quenched by the addition of ice. The obtained solid was filtered and washed with water and MeOH to give intermediate **i-d** as a yellow solid (250 mg, 97%). ^{1}H NMR (400 MHz, $CDCl_3$, TMS, δ): 8.12 (d, J = 8.8 Hz, 1H), 8.08 (s, 1H), 7.66-7.70 (m, 2H), 7.57 (d, J = 8.4 Hz, 1H), 7.49-7.52 (m, 4H), 7.22-7.30 (m, 11H), 7.03-7.05 (m, 3H), 3.18 (s, 1H). This compound was used without further purification.

Intermediate **i-d** (154 mg, 0.200 mmol), **i-c** (129 mg, 0.200 mmol), CuI (4 mg, 0.02 mmol), PPh_3 (11 mg, 0.04 mmol), and $Pd(PPh_3)_4$ (23 mg, 0.02 mmol) were placed in a test tube with screw cap and dissolved with piperidine (4 mL), and the resulting mixture was stirred at 110 ºC for 12 h. After being cooled to room temperature, the reaction mixture was filtered over celite with $CHCl_3$ as an eluent. After removal of the solvent under reduced pressure, the residue was purified by column chromatography on silica gel (hexane:CH_2Cl_2 = 2:1), followed by purification with preparative GPC ($CHCl_3$) to give **PBIT(3Th)-A-PBIT(3Th)** as a yellow solid (171 mg, 68%). ^{1}H NMR (400 MHz, $CDCl_3$, TMS, δ): 8.17-8.19 (m, 4H), 7.79 (dd, J = 8.8, 1.6 Hz, 2H), 7.73 (d, J = 8.8 Hz, 2H), 7.59 (d, J = 8.8 Hz, 2H), 7.51-7.53 (m, 8H), 7.24-7.33 (m, 22H), 7.05 (dd, J = 5.2, 3.6 Hz, 6H); ^{13}C NMR (100 MHz, $CDCl_3$, δ): 156.6, 151.1, 143.9, 142.6, 141.6, 138.5, 137.8, 133.8, 133.4, 133.0, 132.3, 129.2, 128.5, 128.0, 127.9, 126.4, 126.1, 125.8, 124.9, 124.8, 124.6, 124.4, 123.6, 123.1, 120.9, 119.0, 90.6, 63.8; MS (MALDI) *m/z* 1263.94 (M^+, Calcd 1263.73). HRMS (APCI) *m/z*: $[M]^+$ calcd for $C_{80}H_{46}S_8$, 1262.1365; found, 1262.1305.

4.2. MCBJ Method

Polished phosphor-bronze plates (dimensions: 1.6 mm × 0.5 mm, thickness: 0.1 mm) were used as bending beams. Polyimide layers with a thickness of 100 µm were formed by spin-coating commercial poly(pyromellitic dianhydride-*co*-4,4′-oxydianiline) in an amic acid solution (Sigma-Aldrich) followed by baking at 300 °C for 2 h. A pair of Au (30 nm)/Cr (5 nm) electrodes with a spacing of 4 µm were formed on the polyimide film by conventional photolithography. The spacing between the Au electrodes was narrowed by the electrodeposition of Au from an electrolyte solution (TEMPELEX 8400, Electroplating Engineers of Japan, Ltd.) to form a contact between the molecule and the electrodes. The formation of the Au contact was detected by using the technique reported by Liu *et al.*[24]

For the MCBJ measurements, the bending beam was bent from below by a pushing rod driven by a piezoelectric stepper motor (ANPz-51, attocube). The displacement of the electrodes induced by a single step of the piezoelectric stepper motor was estimated to be ~0.04 nm from the tunneling decay constant measured without the molecules.[25] Triangular voltage waves were generated from a digital-to-analog converter (National Instruments, PXI-4461) and were applied to the junction to measure the *I*–*V* characteristics. The electric current was measured using a current amplifier (FEMTO DLPCA-200). The output of the current amplifier was recorded using the analog-to-digital converter (National Instruments, PXI-4461). The MCBJ instrument was placed in the variable-temperature insert of a cryostat (Oxford Instruments) and was cooled by N_2 gas evaporated from liquid N_2. The temperature was monitored by a Si diode sensor attached to the variable temperature insert unit.

4.3. Vector-based Classification

As the feature values for the unsupervised clustering of *I*–*V* curves, we adopted the vector-based properties[21],

$$\Delta X_i = |\mathbf{Y}_i| = |\mathbf{I}_i - \mathbf{R}|, \quad (1)$$

$$\cos(\theta_i) = -\frac{\mathbf{R}\cdot\mathbf{Y}_i}{|\mathbf{R}|\cdot|\mathbf{Y}_i|}, \quad (2)$$

where $\mathbf{I}_i$ is the *i*th current data ranging from –1.5 to 1.5 V and **R** is a reference vector. We used the averaged current as **R**. Before clustering, every data point was normalized such that $|I_{\max,i}| = 1$, where $I_{\max,i}$ is the maximum current value of $\mathbf{I}_i$. Without the normalization, ΔX_i will be dominated by the difference in the conductance because the electric current varies significantly between the data. Furthermore, the order of the elements of $\mathbf{I}_i$ was reversed when the voltage giving $I_{\max,i}$ was negative. In other words, $I_{\max,i}$ always occurred at a positive voltage after normalization. This operation corresponds to unifying the molecular orientations

of the break junction structures. The above normalization enables us to extract the difference in the "shape" of the *I*–*V* curves as feature values.

4.4. First-principles Calculations

The transport properties of the molecules were calculated using the SMEAGOL code[26-28] that is based on the SIESTA package.[29] SMEAGOL employs the non-equilibrium Green's function method combined with DFT. Single/double-zeta plus polarization basis sets were used for the Au/other atoms. The core electrons were described by the Troullier–Martins norm-conserving pseudopotential[30] with the Kleinman–Bylander nonlocal projector.[31] We used the Perdew–Burke–Ernzerhof [32] exchange-correlation functional. Further, the van der Waals interaction was included via Grimme's D2 scheme.[33] Au(111) slabs with *p*(6×6) and *p*(12×6) periodicities were used to model the self-standing and other junction structures, respectively. The *k* points were sampled by 2×2×1 and 1×2×1 grids for the *p*(6×6) and *p*(12×6) slabs, respectively. Denser *k*-point grids (8×8×1 and 4×8×1) were used to calculate the transmission coefficients.

Supporting Information
Supporting Information is available from the Wiley Online Library or from the author.

Acknowledgements
This work was supported by JSPS KAKENHI (20H02814, 20K21224, 20H05841, 20KK0123, 18H03899, 17H03033, 19K15505, and 20H04639), "Dynamic Alliance for Open Innovation Bridging Human, Environmental and Materials", and CREST (J205101030). Thanks are extended to the CAC, ISIR, Osaka University, for assistance in obtaining elemental analyses and HRMS measurements.

Received: ((will be filled in by the editorial staff))
Revised: ((will be filled in by the editorial staff))
Published online: ((will be filled in by the editorial staff))

References

[1] A. Aviram, M. A. Ratner, *Chem. Phys. Lett.* **1974,** *29*, 277.

[2] J. C. Cuevas, E. Scheer, *Molecular Electronics: An Introduction to Theory and Experiment*. World Scientific, Singapore, **2010**.

[3] T. A. Gschneidtner, Y. A. D. Fernandez, K. Moth-Poulsen, *J. Mater. Chem. C* **2013,** *1*, 7127.

[4] C. Joachim, J. K. Gimzewski, A. Aviram, *Nature* **2000,** *408*, 541.

[5] K. Moth-Poulsen, T. Bjornholm, *Nat. Nanotechnol.* **2009,** *4*, 551.

[6] H. Song, M. A. Reed, T. Lee, *Adv. Mat.* **2011,** *23*, 1583.

[7] J. M. Tour, *Acc. Chem. Res.* **2000,** *33*, 791.

[8] M. Tsutsui, M. Taniguchi, *Sensors* **2012,** *12*, 7259.

[9] B. Q. Xu, N. J. J. Tao, *Science* **2003,** *301*, 1221.

[10] L. Sun, Y. A. Diaz-Fernandez, T. A. Gschneidtner, F. Westerlund, S. Lara-Avila, K. Moth-Poulsen, *Chem. Soc. Rev.* **2014,** *43*, 7378.

[11] R. M. Metzger, *Chem. Rev.* **2015,** *115*, 5056.

[12] Y. Kim, T. Pietsch, A. Erbe, W. Belzig, E. Scheer, *Nano Lett.* **2011,** *11*, 3734.

[13] S. Fujii, T. Tada, Y. Komoto, T. Osuga, T. Murase, M. Fujita, M. Kiguchi, *J. Am. Chem. Soc.* **2015,** *137*, 5939.

[14] M. Kiguchi, *Appl. Phys. Lett.* **2009,** *95*.

[15] M. Kiguchi, T. Takahashi, Y. Takahashi, Y. Yamauchi, T. Murase, M. Fujita, T. Tada, S. Watanabe, *Angew. Chem. Int. Ed.* **2011,** *50*, 5707.

[16] C. A. Martin, D. Ding, J. K. Sorensen, T. Bjornholm, J. M. van Ruitenbeek, H. S. J. van der Zant, *J. Am. Chem. Soc.* **2008,** *130*, 13198.

[17] S. Y. Quek, M. Kamenetska, M. L. Steigerwald, H. J. Choi, S. G. Louie, M. S. Hybertsen, J. B. Neaton, L. Venkataraman, *Nat. Nanotechnol.* **2009,** *4*, 230.

[18] Y. Ie, T. Hirose, H. Nakamura, M. Kiguchi, N. Takagi, M. Kawai, Y. Aso, *J. Am. Chem. Soc.* **2011,** *133*, 3014.

[19] Y. Ie, K. Tanaka, A. Tashiro, S. K. Lee, H. R. Testai, R. Yamada, H. Tada, Y. Aso, *J. Phys. Chem. Lett.* **2015,** *6*, 3754.

[20] R. Yamada, K. Albrecht, T. Ohto, K. Minode, K. Yamamoto, H. Tada, *Nanoscale* **2018,** *10*, 19818.

[21] M. Lemmer, M. S. Inkpen, K. Kornysheva, N. J. Long, T. Albrecht, *Nat. Commun.* **2016,** *7*, 12922.

[22] S. Bock, O. A. Al-Owaedi, S. G. Eaves, D. C. Milan, M. Lemmer, B. W. Skelton, H. M. Osorio, R. J. Nichols, S. J. Higgins, P. Cea, N. J. Long, T. Albrecht, S. Martín, C. J. Lambert, P. J. Low, *Chem. Eur. J.* **2017,** *23*, 2133.

[23] W. Ding, M. Koepf, C. Koenigsmann, A. Batra, L. Venkataraman, C. F. A. Negre, G. W. Brudvig, R. H. Crabtree, C. A. Schmuttenmaer, V. S. Batista, *J. Chem. Theor. Comput.* **2015,** *11*, 5888.

[24] B. Liu, J. Xiang, J.-H. Tian, C. Zhong, B.-W. Mao, F.-Z. Yang, Z.-B. Chen, S.-T. Wu, Z.-Q. Tian, *Electrochim. Acta* **2005,** *50*, 3041.

[25] J. M. v. Ruitenbeek, A. Alvarez, I. Piñeyro, C. Grahmann, P. Joyez, M. H. Devoret, D. Esteve, C. Urbina, *Rev. Sci. Instrum.* **1996,** *67*, 108.

[26] A. R. Rocha, V. M. Garcia-Suarez, S. Bailey, C. Lambert, J. Ferrer, S. Sanvito, *Phys. Rev. B* **2006,** *73*, 085414.

[27] I. Rungger, S. Sanvito, *Phys. Rev. B* **2008,** *78*, 035407.

[28] T. Ohto, I. Rungger, K. Yamashita, H. Nakamura, S. Sanvito, *Phys. Rev. B* **2013,** *87*, 205439.

[29] J. M. Soler, E. Artacho, J. D. Gale, A. Garcia, J. Junquera, P. Ordejon, D. Sanchez-Portal, *J. Phys.: Condens. Matter* **2002,** *14*, 2745.

[30] N. Troullier, J. L. Martins, *Phys. Rev. B* **1991,** *43*, 1993.

[31] L. Kleinman, D. M. Bylander, *Phys. Rev. Lett.* **1982,** *48*, 1425.

[32] J. P. Perdew, K. Burke, M. Ernzerhof, *Phys. Rev. Lett.* **1996,** *77*, 3865.

[33] S. Grimme, *J. Comput. Chem.* **2006,** *27*, 1787.

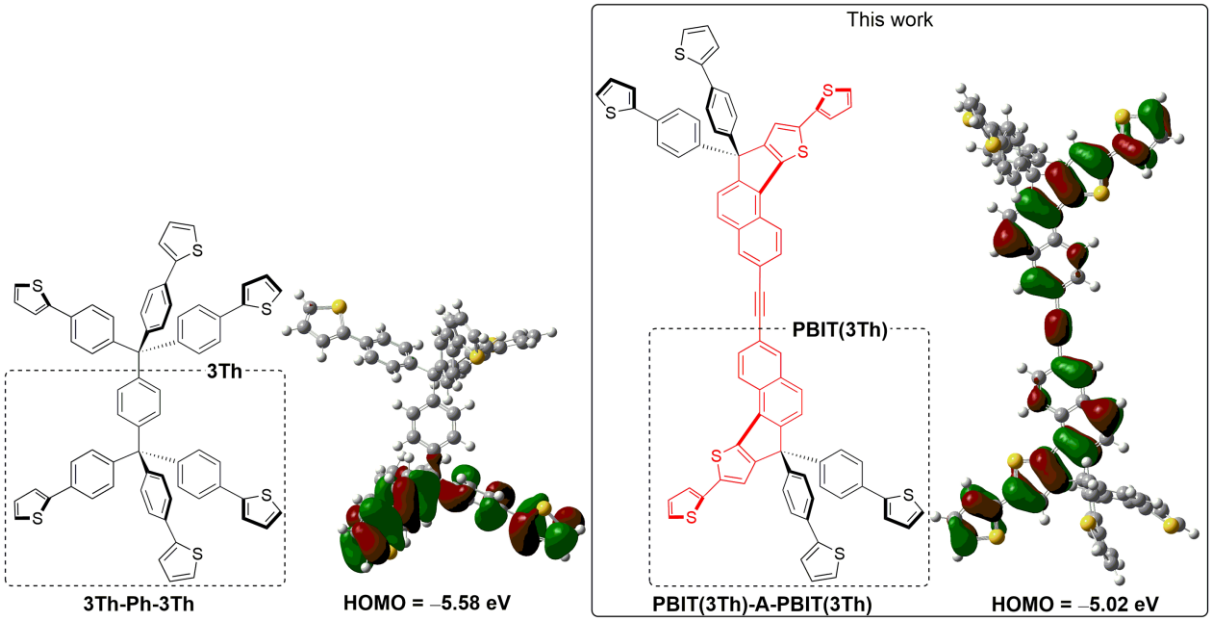

Figure 1. Chemical structures of the tripodal anchor molecules and the HOMO orbitals of their optimized structures.

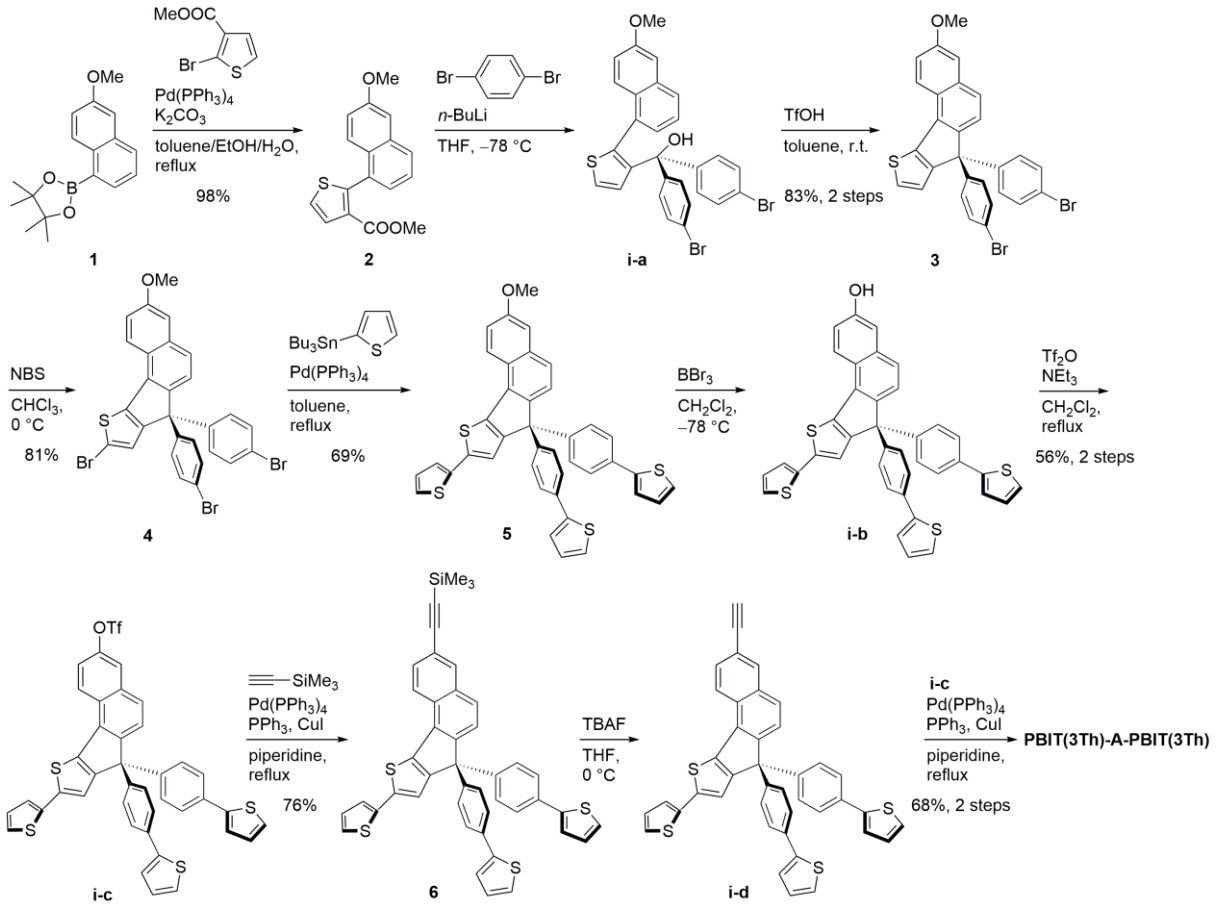

Scheme 1. Synthesis of **PBIT(3Th)-A-PBIT(3Th)**.

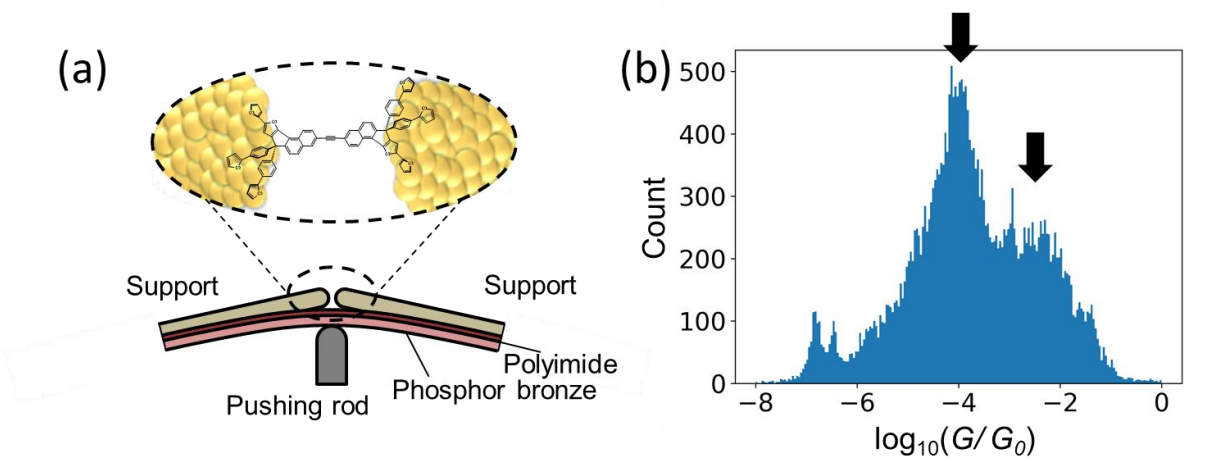

Figure 2. (a) Schematic diagram for the MCBJ measurement and (b) conductance histogram of **PBIT(3Th)-A-PBIT(3Th)**. The arrows indicate the peak conductances.

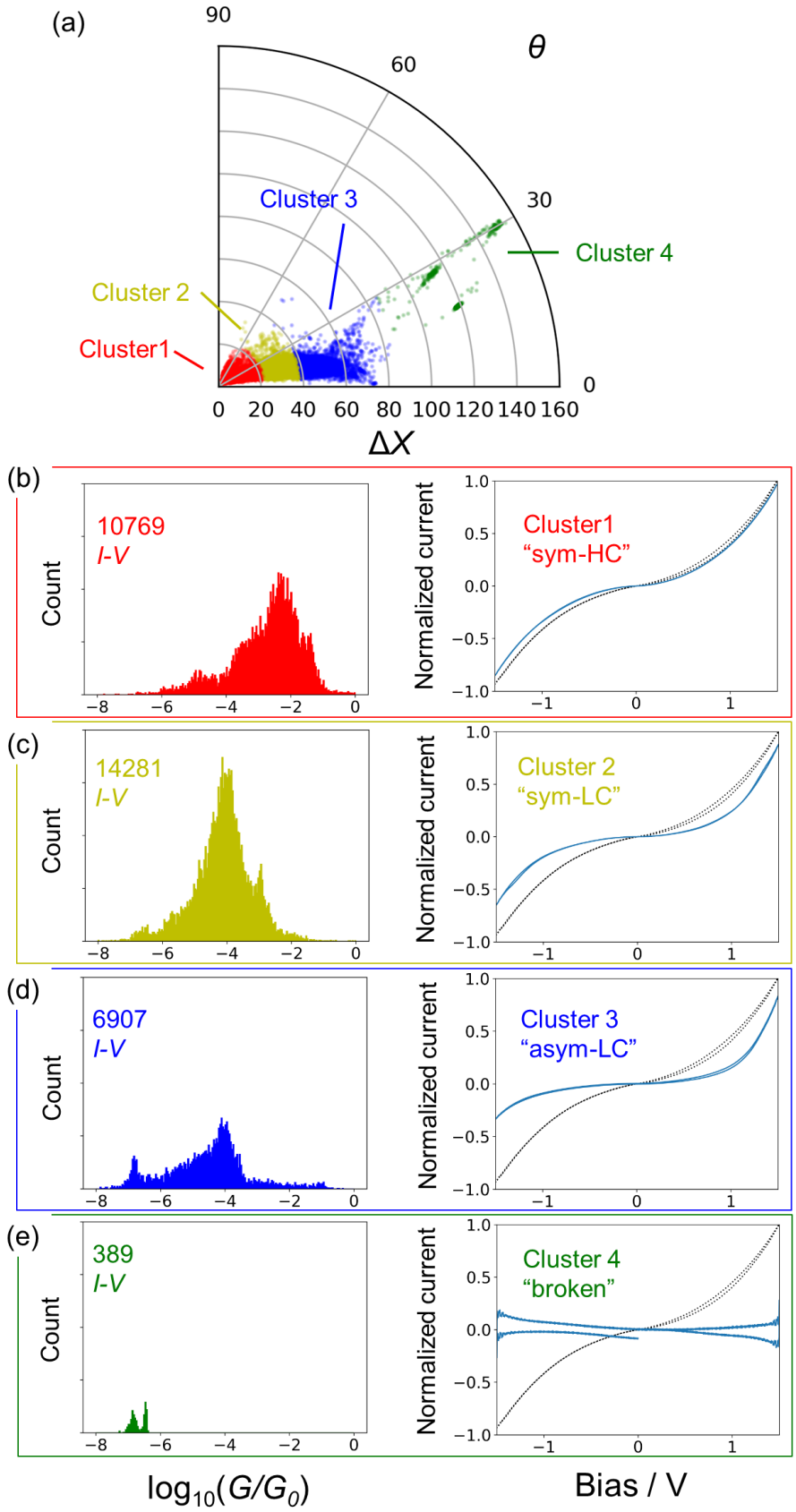

Figure 3. (a) Clusters obtained by vector-based feature values in the k-means clustering method (k = 4). (b)–(e) The normalized *I*–*V* curves averaged within each cluster and the conductance histograms calculated from the *I*–*V* curves (at 100 mV) for clusters 1–4. The reference *I*–*V* curves, **R**, in (b)–(e) are represented by the black dotted lines.

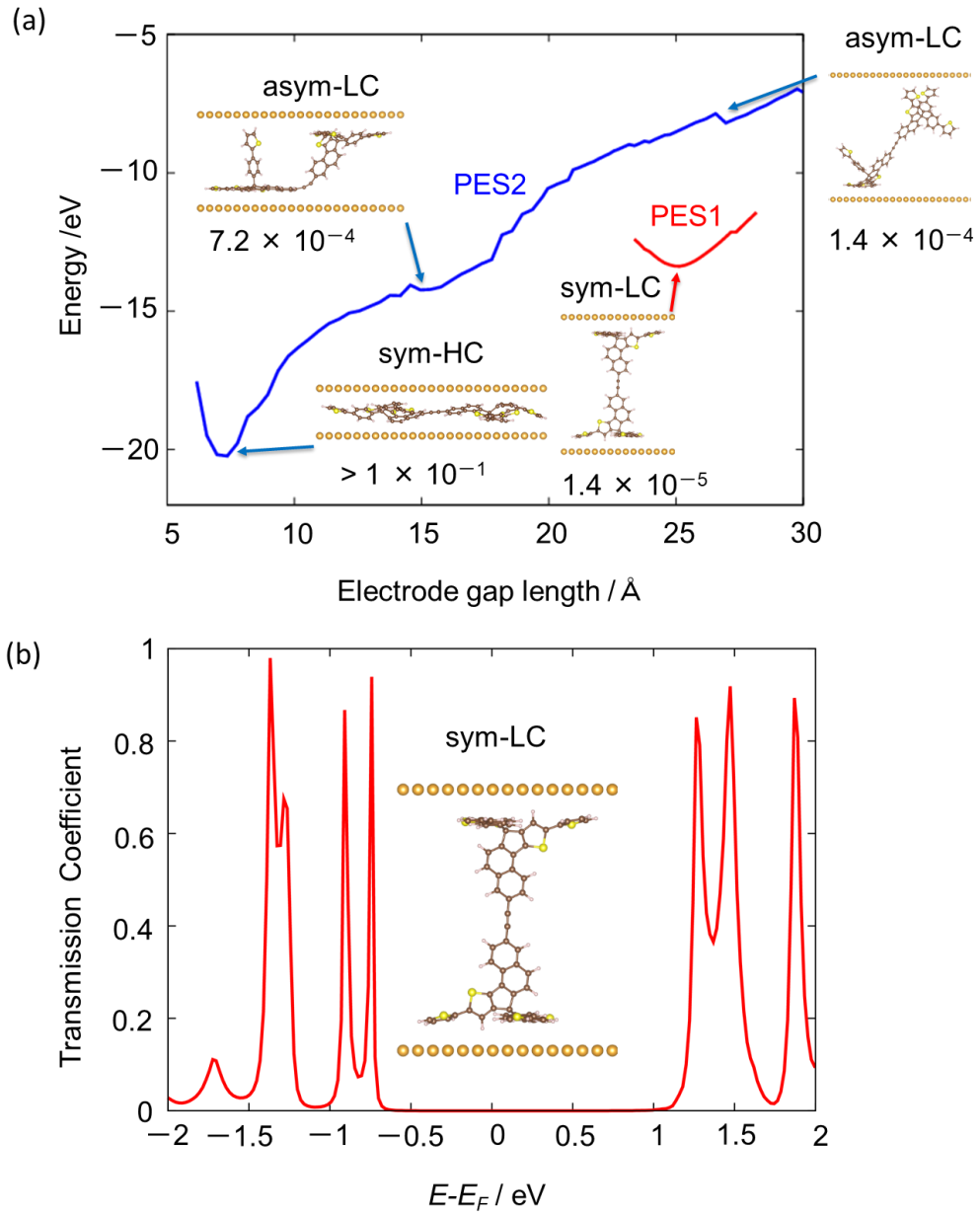

Figure 4. (a) Calculated PES and conductance values for the metastable molecular junction structures. (b) Transmission coefficients of the sym-LC structure.

The table of contents

A tripodal anchor that maintains π-conjugation through an electrode, anchor, and molecular backbone is developed. Single-molecular electrical conductance measurements reveal that this tripodal anchor molecule shows improved electrical conductance. The vector-based classification of the measured *I*–*V* curves together with first-principles transport calculations reveal the transport properties of the tripodal-anchored junction structures.

T. Ohto*, A. Tashiro, T. Seo, N. Kawaguchi, Y. Numai, J. Tokumoto, S. Yamaguchi, R. Yamada*, H. Tada*, Y. Aso* and Y. Ie*

Single-Molecule Conductance of a π-Hybridized Tripodal Anchor while Maintaining Electronic Communication